Linear Ridge Regression with Spatial Constraint for Generation of Parametric Images in Dynamic Positron Emission Tomography Studies

Yun Zhou[1], Sung-Cheng Huang[1], *Senior Member, IEEE*, Marvin Bergsneider[2]
[1]Department of Molecular and Medical Pharmacology, [2]Department of Neurosurgery,
UCLA School of Medicine, Los Angeles, CA 90095

Abstract

Due to its simplicity, computational efficiency, and reliability, weighted linear regression (WLR) is widely used for generation of parametric imaging in positron emission tomography (PET) studies, but parametric images estimated by WLR usually have high image noise level. To improve the stability and signal-to-noise ratio of the estimated parametric images, we have added ridge regression, a statistical technique that reduces estimation variability at the expense of a small bias. To minimize the bias, spatially smoothed images obtained with WLR are used as a constraint for ridge regression. This new algorithm consists of two steps. First, parametric images are generated by WLR and are spatially smoothed. Ridge regression is then applied using the smoothed parametric images obtained in the first step as the constraint. Since both "generalized" ridge regression and "simple" ridge regression are used in statistical applications, we evaluated specifically in this study the relative advantages of the two when incorporated for generating parametric images from dynamic O-15 water PET studies. Computer simulations of a dynamic PET study with the spatial configuration of Hoffman's brain phantom and a real human PET study were used as the data for the evaluation. Results reveal ridge regressions improve image quality of parametric images for studies with high or middle noise level, as compared to WLR. Use of generalized ridge regression offers little advantage over that of simple ridge regression.

I. Introduction

The quantification of a physiological activity based on dynamically acquired PET studies typically requires curve fitting of the measured tissue time-activity curve (TAC). Several strategies have been developed to reduce the random fluctuations in the TAC. One standard method is to draw a large region-of-interest (ROI) and to apply it to the dynamic image set. The averaging of pixel values enclosed within each ROI reduces the noise level in the TAC and therefore improves the accuracy and efficiency of the curve-fitting regression procedure. Using this so-called "ROI method", either Weighted Linear Regression (WLR) or nonlinear regression can be easily and reliably used to estimate model parameters (called micro-parameters) defined in the kinetic model. The inherent drawback to such an approach is that the ROIs must be drawn in advance, a process that may become labor intensive. WLR has been used to estimate micro-parameters in O-15 water dynamic PET studies [1-4] and for the analysis of spatial heterogeneity of Ga-68 EDTA kinetics [5]. For fast generation of myocardial blood flow parametric images with N-13 ammonia PET, a Generalized Linear Least Squares (GLLS) method has also been developed [6].

An often-desired alternative to the above ROI method is the generation of a parametric image representing a given parameter based on modeling the tracer kinetics in tissue for each individual pixel in the image plane. However, applying a model-dependent regression analysis to the pixel-based TAC is fraught with curve-fitting difficulties and with errors secondary to high noise levels. Some of the methodologies developed to overcome these problems have included multiple-time graphical analysis (i.e., "Patlak plot") [7-8] and model-independent linear regression [9]. These techniques, however, are limited to estimating only the macro-parameter (a combination of the micro-parameters of a tracer kinetic model). If micro-parameter estimations are desired, one technique to reduce the pixel value variation is to apply spatial smoothing either to the dynamic images prior to curve-fitting or to the parametric images after the curve-fitting. Spatial smoothing, however, often results in an unacceptable loss in image resolution as well as in enhancing bias errors.

Ridge regression has been used in statistics to reduce estimation variability of linear regressions at the expense of a small bias in the resulted estimates, with the amount of bias dependent on the noise level of the data [10-11]. Also, depending on whether the magnitudes of different parameters are scaled to the same level or not, there are "generalized" and "simple" ridge regressions [12]. We have recently explored the use of ridge regression for generating parametric image from dynamic PET studies. In order to minimize the bias introduced by ridge regression, we used spatially smoothed parametric images obtained from regular WLR as a constraint. So, the procedure consists of two steps. First, parametric images are generated by WLR and are spatially smoothed. In the second step, ridge regression (simple or generalized) is applied using the spatially smoothed parametric images obtained from the first step as the constraint. If simple ridge regression is used, the method is referred to as simple ridge regression with spatial constraint (SRRSC). If generalized ridge regression is used, the method is referred to as generalized ridge regression with spatial constraint (GRRSC). In the present study, we specifically evaluated the relative performance of SRRSC and GRRSC for generation of pixel-based parametric images from dynamic O-15 water PET data. Computer simulations and real PET data were used for the evaluation.

II. Theory and Methods

A. *Theory and Algorithm*

1) Brief Review of Ridge Regression

Ridge regression was introduced by Hoerl and Kennard [10-11] as a method to limit the impact of spurious data in a regression calculation by applying a variable penalty that is dependent on the deviation of data points from the regression line. Starting with the standard linear regression equation:

$$Y = X\beta + e \quad (1)$$

where Y is an nx1 observation matrix, X is an nxm matrix defining the model, e is the measurement noise with E(e)=0 and $E[ee'] = \sigma^2 I_n$, I_n is an n-dimensional identity matrix, and β is an mx1 parameter vector to be estimated. Ridge regression is usually performed in a transformed space by applying an orthogonal transformation T, such that T'T=TT'=I and T'X'XT $= \Lambda$ is diagonal with its diagonal elements $\lambda_1, \lambda_2, \ldots, \lambda_m$ equal to the characteristic root of X'X. By letting

$$\alpha = T'\beta \quad (2)$$

and

$$Z = XT \quad (3)$$

Eq. (1) may be written as

$$Y = Z\alpha + e. \quad (4)$$

Generalized ridge regression finds a parameter vector α_H (Eq. (5) below) and a diagonal H matrix (Eq. (6)) that minimizes the expected mean square error (MSE) of the estimates.

$$\alpha_H = (Z'Z + H)^{-1}Z'Y = (\Lambda + H)^{-1}Z'Y \quad (5)$$

where H is a diagonal matrix with non-negative diagonal elements $h_1, h_2, \ldots, h_m$. A sufficient condition for H to minimize the expected MSE of estimates is:

$$h_i = \sigma^2/\alpha_i^2 \qquad 1 \le i \le m. \quad (6)$$

If we let all diagonal elements of H to be identical, then we have the so-called simple ridge regression estimates:

$$\alpha_h = (Z'Z + hI_m)Z'Y = (\Lambda + hI_m)Z'Y. \quad (7)$$

The variable h is usually selected as

$$h = m\sigma^2/(\alpha'\alpha). \quad (8)$$

In fact, h estimated by Eq. (8) can be viewed as the harmonic mean of the diagonal elements of H in Eq. (6) [12]. Since the true values of σ and α are not known, they are in practice estimated from Eq. (4) by WLR. With H estimated in advance, the ridge regression result can be viewed as the parameter vector that minimizes the following cost function

$$Q(\alpha_H|H) = (Y-Z\alpha_H)'(Y-Z\alpha_H) + \alpha_H'H\alpha_H. \quad (9)$$

2) Ridge Regression with Spatial Constraint

The GRRSC/SRRSC procedure consists of two steps. In the first step, regular WLR is applied to the kinetics of each pixel. The resulted parametric image β is spatially smoothed with a filter S, and the smoothed β is denoted as β_s. The noise variance of the data (σ^2) for each pixel is estimated from the residuals of the WLR. Based on the estimated σ^2 and β, the diagonal ridge matrix H is calculated as

$h_i = \sigma^2/(\beta_i - \beta_{si})2$, $\quad 1 \le i \le m$ for GRRSC, and
$h_i = m\sigma^2/((\beta-\beta_s)'(\beta-\beta_s))$, $\quad 1 \le i \le m$ for SRRSC.

h_i is then also smoothed spatially by filter S.

The second step applies the ridge regression. As shown in the above subsection, ridge regression is equivalent to minimizing a cost function (Eq. (9)). For GRRSC/SRRSC, we seek to minimize the following cost function.

$$Q(\beta|H) = (Y-X\beta)'W(Y-X\beta) + (\beta-\beta_s)'H(\beta-\beta_s), \quad (10)$$

where Y is a measured tissue time activity vector, X is regression coefficient matrix determined by the tracer kinetic model, W is diagonal matrix and its diagonal element w_{ii} is equal to the duration of i^{th} frame of a PET dynamic scanning (i.e., W = diag(w_{ii})). Compared to WLR, the cost function of GRRSC or SRRSC expressed in Eq. (10) includes an additional penalty term. Since the H matrix is proportional to the noise variance of the measured data, the penalty term automatically adjusts for the noise level of the pixel kinetics.

If Eq. (10) is converted to a centralized form by letting $\beta_1 = \beta-\beta_s$, $Y_1 = W_1Y$, and $X_1 = W_1X$ with $W_1 = \text{diag}(w_{ii}^{0.5})$, then the cost function to be minimized becomes

$$Q(\beta_1|H) = (Y_1-X_1\beta_1)'(Y_1-X_1\beta_1) + \beta_1'H\beta_1. \quad (11)$$

and the solution that minimizes the above cost function can be determined to be

$$\beta(H) = (X'WX+H)^{-1}(X'WY + H\beta_s) \quad (12)$$

For SRRSC, it can be further simplified to

$$\beta(h) = (X'WX+hI_m)^{-1}(X'WY + h\beta_s), \quad (13)$$

where m is dimension of parameter vector β and I_m is an m-dimensional identity matrix. It can be seen from the above equations that as H or h tends to zero, GRRSC/SRRSC becomes regular WLR. As h or the minimum of the diagonal elements of H tends to infinity, the results of GRRSC/SRRSC will be β_s, and the bias introduced by GRRSC/SRRSC is limited by the spatial constraint β_s.

B. *Evaluation by Computer Simulation*

The following 2-compartment 3-parameter model was used to generate measured O-15 water tracer kinetics in brain tissue [2, 13, 14]:

$$C_{tot} = C_b(t) + V_0C_a(t) \quad (14)$$

$$\frac{dC_b(t)}{dt} = K_1C_a(t) - k_2C_b(t) \quad (15)$$

where $C_b(t)$ is brain tissue radioactivity, C_{tot} corresponds to the measured tissue time activity from the PET scanner, Ca is arterial whole blood O-15 water time activity, K_1 is cerebral blood flow, k_2 is clearance rate constant. The vascular volume and dispersion constant are lumped as one parameter V_0. To apply linear regression algorithm for model parameter estimation, the unobservable $C_b(t)$ in Eq. (15) can be eliminated by taking the derivative on both sides of Eq. (14) and substituting the derivative of $C_b(t)$ with that in Eq. (15). The result is shown in Eq. (16) below.

$$\frac{dC_{tot}(t)}{dt} = (K_1 + k_2V_0)C_a(t) - k_2C_{tot}(t) + V_0\frac{dC_a(t)}{dt} \quad (16)$$

By applying boundary condition, $C_{tot}(0) = 0$, and $C_a(0) = 0$, to Eq. (16), the integral form of Eq. (16) is given as Eq. (17).

$$C_{tot}(t) = (K_1+k_2V_0)\int C_a ds - k_2\int C_{tot} ds + V_0 C_a \qquad (17)$$

Let $\beta' = [K_1+k_2V_0\ k_2\ V_0]$, then Eq. (17) can be discretized and converted to the form of linear regression model of Eq. (1) as

$$\begin{bmatrix} C_{tot}(t_1) \\ C_{tot}(t_2) \\ \cdot \\ \cdot \\ \cdot \\ C_{tot}(t_n) \end{bmatrix} = \begin{bmatrix} \int_0^{t_1} C_a ds & -\int_0^{t_1} C_{tot} ds & C_a(t_1) \\ \int_0^{t_2} C_a ds & -\int_0^{t_2} C_{tot} ds & C_a(t_2) \\ \cdot & \cdot & \cdot \\ \cdot & \cdot & \cdot \\ \cdot & \cdot & \cdot \\ \int_0^{t_n} C_a ds & -\int_0^{t_n} C_{tot} ds & C_a(t_n) \end{bmatrix} \beta \qquad (18)$$

Three sets of parameters for gray and white matter were used to generate tissue kinetics (see Table 1).

	Gray Matter			White Matter		
	K_1	k_2	V_0	K_1	k_2	V_0
Set_1	0.80	0.84	0.05	0.20	0.25	0.03
Set_2	0.60	0.63	0.05	0.20	0.25	0.03
Set_3	0.40	0.42	0.05	0.20	0.25	0.03

Table 1: Spatial distribution of parameters used in computer simulation. The units of K_1, k_2, V_0 are ml/min/g, 1/min, and ml/g, respectively.

For the phantom study, an arterial blood O-15 water time activity curve from a human study was used as the input function. The simulated dynamic PET scanning sequence was 6x5, 9x10, and 6x30 seconds. The spatial distribution of the gray and white matter follows that of the Hoffman's phantom [15]. Pseudo random noise (normal distributed with variance proportional to its mean) with three different noise levels (higher: $1.25x10^6$, middle: $5x10^6$, lower: $10x10^6$ total counts per plane over 5 minutes) was simulated in the sinogram. Fifty realizations for each noise level were obtained. Dynamic images were reconstructed by filtered back projection (Hanning-filter, 128x128 matrix, pixel size 0.125 cm, cut-off at the Nyquist frequency). 2D linear filters with different sizes (3x3, 5x5, and 7x7: same weighting for all pixels of the filter) were used as the spatial smoothing filter. The true parametric images were reconstructed from a noise-free sinogram. The variance of each parameter estimate at each pixel was defined as percent root MSE,

$$RMSE\% = \frac{100}{p}\sqrt{\frac{\sum_{i=1}^{N}(p - p_i)^2}{N-1}} \qquad (19)$$

where p_i is the parameter estimate, p is the true value reconstructed from the noise-free sinogram and N is the number of repeated realizations. In addition, the pixel-wise mean, bias, square of bias, variance, and MSE of the estimated parametric images were also calculated for each parameter and for each pixel. The ROI average RMSE%, square of bias, and variance for gray and white matter were calculated from each corresponding image for the three methods: WLR, SRRSC, and GRRSC.

C. *Human O-15 Water PET Dynamic Study*

A single study obtained on a control subject was utilized for this analysis. A single bolus of O-15 water (15 mCi) was injected intravenously. Dynamic PET scans obtained using a Siemens/CTI EXACT HR+ scanner were obtained using the following acquisition sequence: 6x5, 9x10, 6x30 sec.(total 5 minutes, 21 frames). The data were collected in 3-D acquisition mode. The dynamic images were reconstructed using filtered backprojection with Hanning 0.5 and 0.3 filters for evaluating the noise level effects on the parametric images (63 planes, matrix size 128x128, pixel size 0.1446 cm, plane separation 0.2425 cm). Arterial whole blood was sampled during the scan and activity measured in a well counter to give the input function. The Eq. (18) was used to fit the measured time activity curves by WLR, GRRSC and SRRSC methods. The smoothing filter used to smooth parametric images generated by WLR was a 2-D linear filter of 5x5 in size.

The correction of input function delay was performed before parametric imaging. In dynamic PET study, there is a time delay between the peripherally sampled input function and the brain tissue radioactivity measurement due to the systematic time difference between the tracer arrival times in the brain relative to the peripheral sampling site. For $H_2{}^{15}O$ dynamic PET study, the delay of the input function may produce a non-negligible error in the model parameter estimation. The fast determination of input function delay by linear regression method [2] was used in the present study to estimate a global time delay value.

III. Results and Discussions

A. *Simulation Results*

Table 2 is the average of RMSE% of gray matter, white matter, and whole brain for 3 data sets and 3 noise levels. The smoothing filter with 5x5 window was used in SRRSC and GRRSC. Multivariate analysis of variance (MANOVA) reveals that the RMSE% for the SRRSC and GRRSC estimates are significantly lower than those based on WLR estimates (at p=0.01 level). The improvement of estimate accuracy by SRRSC or GRRSC decreases as the noise level lessens. The RMSE% of estimates are about 35% less at high noise level and 15% less at lower noise level with GRRSC and SRRSC as compared to those with WLR for all three data sets. The MANOVA analysis also reveals that there is no essential difference between SRRSC and GRRSC in terms of the RMSE%.

The SRRSC and GRRSC methods are not sensitive to the smoothing filter used on the parameters estimated by WLR. The average RMSE% as a function of smoothing filter is

shown in Table 3. There is a nonlinear relationship between the RMSE% and smoothing filter used. In this limited analysis, the smoothing filter with a 5x5 window gives the lowest RMSE%. Fortunately, neither SRRSC nor GRRSC is sensitive to the smoothing filter used.

The MSE consists of bias and variance components. Table 4 is a summary of MSE analysis for the three methods. Table 4 shows that the magnitude of bias of estimates increases as noise level increases for WLR, SRRSC, and GRRSC. Theoretically WLR estimates is not biased while GRRSC and SRRSC estimates are biased. However, due to model approximation, measurement errors, the estimates are generally biased [3]. In the present study, we found that both SRRSC and GRRSC have more reduction in variance by increasing a little bias, so MSE is decreased. In fact, the variance of GRRSC and SRRSC estimates are decreased by ridge regression while the bias of estimates of SRRSC and GRRSC is limited by the spatial constraint.

B. Human Study Results

Consistent with the simulation studies, both SRRSC and GRRSC provided better image quality for O-15 water study. Figure 1 shows the CBF images estimated by WLR, SRRSC, and GRRSC for the one control study. The CBF parametric images generated by SRRSC and GRRSC are comparable based on visual inspection. The corresponding pixel values of the parametric images derived from the GRRSC and SRRSC methods were highly correlated:

$$GRRSC(K_1) = 0.97SRRSC(K_1) + 0.0093 \qquad (20)$$

with $R^2 = 0.99$. The CBF parametric images for the dynamic images reconstructed with hanning-0.3 filter is shown at the bottom of Figure 1. As the noise level is reduced by the use of a lower cutoff filter (hanning-0.3) in the image reconstruction, the differences among the three methods become small.

IV. Summary and Conclusion

Computer simulation and human dynamic PET studies reveal that both SRRSC and GRRSC improved parametric images quality for studies with high or middle noise level of, as compared to WLR. GRRSC offers no significant improvement in the parametric images as compared to SRRSC. For its lower computational burden and its simplicity, SRRSC should be considered as a method of choice for generating parametric images for O-15 dynamic studies.

V. Acknowledgments

This work was partially supported by DOE contract DE-FC03-87ER60605 and NIH grant NS30308-06A2.

			Gray matter			White matter			whole brain		
			K_1	k_2	V_0	K_1	k_2	V_0	K_1	k_2	V_0
set_1	high noise	WLR	43.5	50.2	242.1	72.7	123.3	296.2	52.4	76.0	248.8
		SRRSC	28.2	32.1	179.8	44.7	72.5	218.5	33.0	46.1	184.2
		GRRSC	29.6	36.2	160.7	48.5	83.4	198.7	35.3	52.5	166.0
	middle noise	WLR	22.5	30.4	123.4	34.7	61.5	150.0	26.0	40.9	126.4
		SRRSC	16.9	23.0	97.6	24.6	42.0	116.2	18.9	29.1	99.0
		GRRSC	17.1	25.1	84.9	26.0	46.6	102.9	19.6	32.1	86.9
	low noise	WLR	16.0	24.2	87.8	24.6	43.5	106.1	18.4	30.4	89.7
		SRRSC	13.2	20.1	73.1	18.9	32.5	85.6	14.6	23.8	73.6
		GRRSC	12.9	21.3	61.8	19.5	35.1	74.1	14.7	25.5	62.9
set_2	high noise	WLR	43.5	56.9	210.8	68.0	120.1	269.2	50.5	78.4	221.1
		SRRSC	26.9	35.2	151.0	40.8	69.6	194.9	30.8	46.7	159.4
		GRRSC	28.9	40.0	137.4	44.4	80.1	176.9	33.3	53.4	144.7
	middle noise	WLR	21.8	33.0	106.9	32.1	59.6	135.8	24.6	41.5	111.9
		SRRSC	15.2	23.8	80.3	21.5	38.7	102.1	16.8	28.3	84.1
		GRRSC	16.0	26.4	72.2	23.1	43.6	91.2	17.8	31.6	75.4
	low noise	WLR	15.3	25.8	75.8	22.4	42.2	95.7	17.2	30.7	79.1
		SRRSC	11.6	20.4	59.3	16.0	29.6	74.5	12.6	22.8	61.7
		GRRSC	11.8	22.1	52.4	16.9	32.7	65.4	13.1	24.9	54.3
set_3	high noise	WLR	44.3	72.1	174.8	60.7	113.8	234.6	48.1	84.1	187.8
		SRRSC	26.6	43.0	122.0	35.7	65.0	167.4	28.6	49.1	132.5
		GRRSC	28.8	49.0	112.4	38.7	74.6	151.2	30.9	56.2	120.9
	middle noise	WLR	21.7	39.7	88.0	29.2	56.7	118.3	23.4	44.0	94.6
		SRRSC	14.1	26.9	63.1	18.5	34.9	85.9	15.0	28.4	68.3
		GRRSC	15.3	30.3	58.4	19.9	39.6	77.8	16.2	32.2	62.5
	low noise	WLR	15.4	30.2	62.2	20.5	40.3	83.9	16.4	32.4	67.0
		SRRSC	10.5	22.2	45.8	13.4	25.8	61.7	11.0	22.3	49.3
		GRRSC	11.3	24.7	42.3	14.4	29.3	55.6	11.8	25.0	45.0

Table 2: Average RMSE% of gray matter, white matter, and whole brain for 3 data sets and 3 noise levels .The smoothing filter with 5x5 window was used in SRRSC and GRRSC.

		Gray matter			White matter			whole brain		
		K_1	k_2	V_0	K_1	k_2	V_0	K_1	k_2	V_0
SRRSC	3x3	16.9	23.8	96.6	25.8	44.7	116.8	19.4	30.6	98.7
	5x5	16.9	23.0	97.6	24.6	42.0	116.2	18.9	29.1	99.0
	7x7	17.9	23.9	101.7	25.7	43.6	119.3	19.9	30.2	102.5
GRRSC	3x3	17.6	25.4	90.8	27.0	47.6	110.9	20.3	32.6	93.2
	5x5	17.1	25.1	84.9	26.0	46.6	102.9	19.6	32.1	86.9
	7x7	17.6	25.7	84.8	26.8	48.4	101.8	20.2	33.1	86.4

Table 3: Average of RMSE% for SRRSC and GRRSC using filters with 3x3, 5x5, and 7x7 smoothing windows. RMSE% was based on set_1 simulation data with middle noise level.

Noise level	Fitting methods	K_1			k_2			V_0		
		$(bias)^2$	variance	MSE	$(bias)^2$	variance	MSE	$(bias)^2$	variance	MSE
High	WLR	0.0017	0.0641	0.06578	0.0075	0.1127	0.1204	0.0002	0.0099	0.0102
	SRRSC	0.0030	0.0239	0.0270	0.0070	0.040	0.0473	0.0003	0.0052	0.0056
	GRRSC	0.0019	0.0285	0.0304	0.0076	0.0524	0.0601	0.0002	0.0044	0.0046
Middle	WLR	0.0007	0.0160	0.0167	0.0090	0.0293	0.0386	0.0001	0.0025	0.0026
	SRRSC	0.0018	0.0074	0.0092	0.0079	0.0132	0.0213	0.0001	0.0015	0.0016
	GRRSC	0.0011	0.0085	0.0096	0.0087	0.0166	0.0255	0.0000	0.0012	0.0012
Low	WLR	0.0006	0.0078	0.0085	0.0088	0.0146	0.0237	0.0000	0.0013	0.0013
	SRRSC	0.0016	0.0041	0.0057	0.0082	0.0075	0.0159	0.0000	0.0009	0.0009
	GRRSC	0.0009	0.0046	0.0055	0.0088	0.0091	0.0181	0.0000	0.0006	0.0006

Table 4: Whole brain average of MSE components analysis based on data set_1 simulations.

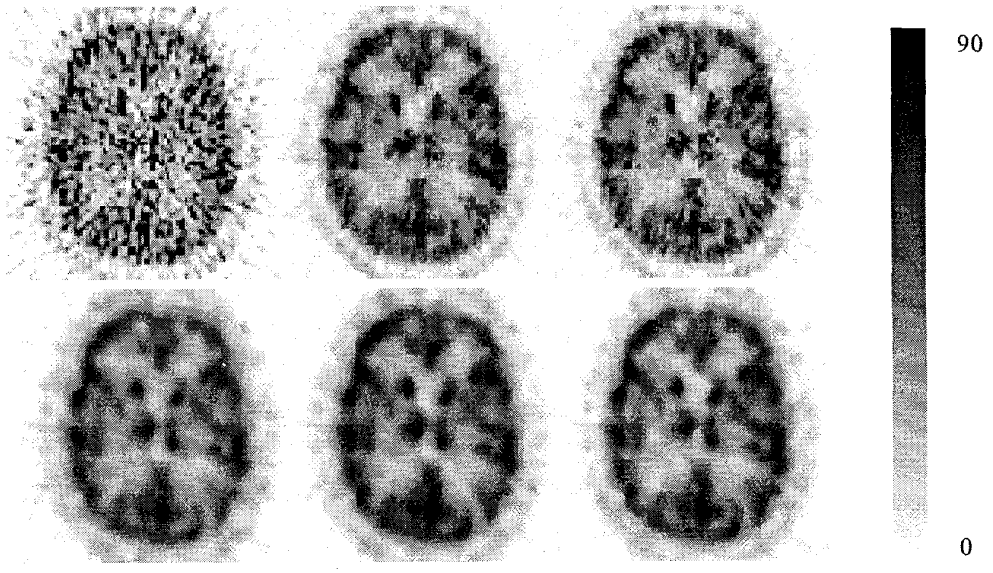

Figure 1. CBF (ml/min/100g) images estimated by WLR (left), SRRSC (middle), and GRRSC (right) from dynamic images reconstructed with hanning-0.5 (upper row) and hanning-0.3 (lower row) in a human study.

VI. REFERENCES

[1] R. E. Carson, S.-C. Huang, and M. V. Green, "Weighted integration method for local cerebral blood flow measurements with positron emission tomography," *J. Cereb. Blood Flow Metab*., vol. 6, pp. 245-258, 1986.

[2] J. V. Hoff, W. Burchert , W. Muller-Schauenburg, G.-J. Meyer and H. Hundeshagen, "Accurate local blood flow measurements with dynamic PET: fast determination of input function delay and dispersion by multilinear minimization," *J. Nucl. Med.* vol. 32,pp. 733-738, 1991.

[3] D. Fang, Z. Wang, and S.-C. Huang, "A study on statistically reliable and computationally efficient algorithms for generating local cerebral blood flow parametric images with positron emission tomography," *IEEE Transactions on Medical Imaging*, vol. 12, pp.182-188, 1993.

[4] T. Yokoi, H. Iida, H. Itoh and I. Kanno, "A new graphic plot analysis for cerebral blood flow and partition coefficient with Iodine-123-Iodoamphetamine and dynamic SPECT validation studies using Oxygen-15-Water studies and PET," *J. Nucl. Med.* vol. 34, pp. 498-505, 1993.

[5] Y. Zhou, S.-C. Huang, T. Cloughesy, C.K. Hoh, K. Black, M. E. Phelps, "A modeling-based factor extraction method for determining spatial heterogeneity of Ga-68 EDTA kinetics in brain tumors," *IEEE Transactions on Nuclear Science*, vol. 44, pp. 2522-2527, 1997.

[6] K. Chen, M. Lawson, E. Reiman, A. Cooper, D. Feng, S.-C. Huang, D. Bandy, D. Ho, "Generalized linear least squares method for fast generation of myocardial blood flow parametric images with N-13 Ammonia PET," *IEEE Transactions on Medical Imaging*, vol. 17, pp. 236-243, 1998.

[7] C. S. Patlak, R. G. Blasber, and J. D. Fenstermacher, "Graphical evaluation of blood-to-brain transfer constants from multiple-time uptake data," *J. Cereb. Blood Flow Metab*. vol 3, pp. 1-7, 1983.

[8] C. S. Patlak, R. G. Blasber, and J. D. Fenstermacher, "Graphical evaluation of blood-to-brain transfer constants from multiple-time uptake data, Generalizations," *J. Cereb. Blood Flow Metab*. vol 5, pp. 584-590, 1985.

[9] J. A. Thie, G. T. Smith, and K. F. Hubner, "Linear least squares compartment-model-independent parameter identification in PET," *IEEE Transactions on Medical Imaging*, vol. 16, pp. 11-16, 1997.

[10] A. E. Hoerl and R. W. Kennard, "Ridge regression: biased estimation for nonorthogonal problems," *Technometrics*, vol. 12, pp. 55-67, 1970.

[11] A. E. Hoerl and R. W. Kennard, "Ridge regression: applications to nonorthogonal problems," *Technometrics*, vol. 12, pp. 69-82,1970.

[12] A. E. Hoerl, R. W. Kennard, and K. F. Baldwin, "Ridge regression: Some simulations," *Commun. Statis.-Theor. Meth*., vol. 4, pp. 105-123, 1975.

[13] K. S. St. Lawrence; T. Y. Lee. "An adiabatic approximation to the tissue homogeneity model for water exchange in the brain: II. Experimental validation," *J. Cereb. Blood Flow Metab.* vol. 18, pp. 1378-85, 1998.

[14] K. S. St. Lawrence; T. Y. Lee, "An adiabatic approximation to the tissue homogeneity model for water exchange in the brain: I. Theoretical derivation," *J. Cereb. Blood Flow Metab*, vol. 18, pp. 1365-77, 1998.

[15] E. J. Hoffman, A. R. Ricci, L. M. A. M. van der Stee, M. E. Phelps, "ECAT III – basic design considerations," *IEEE Transactions on Nuclear Scienc,* NS-30, pp. 729-733, 1983.